Combustion Science and Technology

ISSN: 0010-2202 (Print) 1563-521X (Online) Journal homepage: www.tandfonline.com/journals/gcst20

Analytical and Numerical Investigations of Wedge-Induced Oblique Detonation Waves at Low Inflow Mach Number

Yan Liu, Dan Wu, Songbai Yao & Jianping Wang

To cite this article: Yan Liu, Dan Wu, Songbai Yao & Jianping Wang (2015) Analytical and Numerical Investigations of Wedge-Induced Oblique Detonation Waves at Low Inflow Mach Number, Combustion Science and Technology, 187:6, 843-856, DOI: 10.1080/00102202.2014.978865

To link to this article: https://doi.org/10.1080/00102202.2014.978865

Combust. Sci. Technol., 187: 843–856, 2015

ISSN: 0010-2202 print / 1563-521X online
DOI: 10.1080/00102202.2014.978865

Taylor & Francis
Taylor & Francis Group

ANALYTICAL AND NUMERICAL INVESTIGATIONS OF WEDGE-INDUCED OBLIQUE DETONATION WAVES AT LOW INFLOW MACH NUMBER

Yan Liu, Dan Wu, Songbai Yao, and Jianping Wang

Center for Combustion and Propulsion, CAPT and SKLTCS, Department of Mechanics and Engineering Science, College of Engineering, Peking University, Beijing, China

The wedge-induced oblique detonation wave (ODW) at low inflow Mach number is investigated via Rankine–Hugoniot analysis and numerical simulations. The results show that the Chapman–Jouguet oblique detonation wave (CJ ODW) plays a significant role in the structure of the ODW. And the influence of the CJ ODW is the reason why an attached ODW can propagate upstream. Both the analytical and numerical results show that the decrease of inflow Mach number and the increase of wedge angle are conducive to the upstream propagation of ODW. In the upstream propagation process, a Mach reflection wave configuration is always established on the wedge surface. For the upstream propagating ODW that cannot detach from the wedge surface by itself, it will stabilize at a point on the wedge surface with an induction region, which is a few times the length of the induction zone of an ideal Zeldovich–von Neumann–Döring (ZND) detonation. Benefiting from the short induction region, the stabilized upstream propagating ODW has extraordinary stability.

Keywords: CJ ODW; Numerical simulation; Oblique detonation wave; Rankine–Hugoniot analysis

INTRODUCTION

An oblique detonation wave (ODW) stabilized in the supersonic flow of premixed detonable gas over a wedge has received much attention in the past decades. As a promising potential combustion mechanism of supersonic propulsion systems, such as the ram accelerator (Brackett and Bogdanoff, 1989; Grismer and Powers, 1995) and the ODW engine (Cambier et al., 1988; Dudebout et al., 1998), extensive analytical, experimental, and numerical investigations on the ODW have been performed.

The detailed structure of the ODW induced by a wedge was numerically investigated by Li et al. (1994). The oblique shock wave (OSW), the induction region, and the ODW were revealed in their work and then observed in the experiments performed by Viguier et al. (1996), Morris et al. (1998), and Verreault and Higgins (2011). Through numerical and experimental investigations, Verreault and Higgins (2011) and Verreault et al. (2012, 2013) proposed that the induction region was ended by a set of compression waves that were

Received 22 April 2014; revised 9 October 2014; accepted 16 October 2014.

Address correspondence to Yan Liu, Center for Combustion and Propulsion, CAPT and SKLTCS, Department of Mechanics and Engineering Science, College of Engineering, Peking University, Beijing 100871, China. E-mail: liuyandeyoux@126.com

Color versions of one or more of the figures in the article can be found online at www.tandfonline.com/gcst.

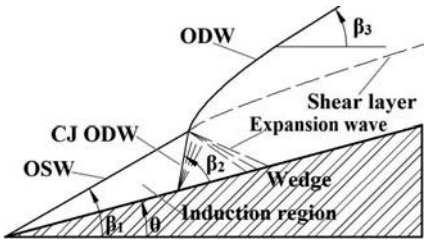

Figure 1 Schematic of the ODW structure suggested by Ghorbanian and Sterling (1996). β_1: the OSW angle; β_2: the CJ ODW angle; β_3: the ODW angle.

sent from the exothermic reactions. In the experimental and numerical results presented by Desbordes et al. (1995), Viguier et al. (1996) and Maeda et al. (2012), the induction region was observed to be followed by a detonation wave, and the corresponding detonation pressure signal was obtained experimentally by Dabora and Broda (1993). In the model proposed by Ghorbanian and Sterling (1996), the induction region was ended by a Chapman–Jouguet oblique detonation wave (CJ ODW), which was identical to the analytical result of Ashford and Emanuel (1994). In order to distinguish from the above mentioned ODW, which could be either overdriven or at the CJ state (Pratt et al., 1991), the detonation wave at the end of the induction region was called a CJ ODW (Ghorbanian and Sterling, 1996; Verreault et al., 2012), since it is always at the CJ state. The corresponding wave structure is illustrated in Figure 1, in which the OSW angle β_1, the CJ ODW angle β_2, and the ODW angle β_3 are defined. β_1 denotes the angle between the OSW and the upstream flow. β_2 denotes the angle between the CJ ODW and the wedge surface. β_3 denotes the angle between the ODW and the upstream flow.

Besides the structure, the stability of the ODW has also been investigated extensively. A periodic instability of the triple-point of the ODW induced by a wedge with large induction time was observed in the experiments conducted by Viguier et al. (1998). According to the state of stability, Gui et al. (2011) divided the ODW into three sections: Zeldovich–von Neumann–Döring (ZND) model-like structure, single-sided triple point structure, and dual-headed triple point structure. The origin of the right-running transverse wave of the dual-headed triple point structure was revealed by Verreault et al. (2013). They found that the formation of the right-running transverse wave resulted from the temporal instability of the spatial oscillations of the oblique shock wave. According to the numerical simulations performed by Choi et al. (2009), with detached conditions of ODW identical to Morris et al. (1998), the decoupling between the reaction front and the OSW may result in an attached periodical oscillating oblique shock-induced combustion. In the numerical simulations performed by Li et al. (1994) and Teng et al. (2007), the stability of ODW at high and critical inflow Mach number was confirmed. An upstream propagating ODW induced by a conical blunt body was presented by Lefebvre and Fujiwara (1995). They found that the upstream propagating ODW eventually stabilized at the leading edge of the blunt body. The upstream propagating ODW induced by a wedge was also obtained in the numerical simulations of Figueira da Silva and Deshaies (2000).

In the cases of an upstream propagating ODW, the length of the induction region decreased dramatically (Lefebvre and Fujiwara, 1995). According to the numerical results presented by Papalexandris (2000), to effectively trigger an ODW, the adopted wedge should be longer than the induction region. Therefore, the wedge length needed for the upstream propagating ODW can be significantly reduced. This is a very desirable

feature for propulsion applications. Thus, a detailed investigation on this problem would be significant and helpful in the applications of ODW to propulsion. In this article, both Rankine–Hugoniot (R–H) analysis and numerical simulations are performed to investigate the mechanism and stability of the upstream propagating ODW.

NUMERICAL METHOD AND PHYSICAL MODEL

In this study, the effects of viscosity, thermal conduction, and mass diffusion are assumed to be negligible. The two-dimensional Euler equations coupled with a two-step chemical reaction model (Korobeinikov et al., 1972) are adopted to simulate the OSW and the ODW over a planar wedge. The governing equations are summarized as follows:

$$\frac{\partial \boldsymbol{U}}{\partial t}+\frac{\partial \boldsymbol{E}}{\partial x}+\frac{\partial \boldsymbol{F}}{\partial y}=\boldsymbol{S} \tag{1}$$

$$\boldsymbol{U}=\begin{bmatrix}\rho\\ \rho u\\ \rho v\\ e\\ \rho\beta\\ \rho\alpha\end{bmatrix},\ \boldsymbol{E}=\begin{bmatrix}\rho u\\ \rho u^2+p\\ \rho uv\\ (e+p)u\\ \rho u\beta\\ \rho u\alpha\end{bmatrix},\ \boldsymbol{F}=\begin{bmatrix}\rho v\\ \rho uv\\ \rho v^2+p\\ (e+p)v\\ \rho v\beta\\ \rho v\alpha\end{bmatrix},\ \boldsymbol{S}=\begin{bmatrix}0\\ 0\\ 0\\ 0\\ \rho\omega_\beta\\ \rho\omega_\alpha\end{bmatrix} \tag{2}$$

where ρ, p, u, and v are the density, static pressure, and velocity components in the x and y directions, respectively. E is the total energy per unit volume:

$$e=\frac{p}{\gamma-1}+\beta\rho q+\frac{1}{2}\rho u^2+\frac{1}{2}\rho v^2 \tag{3}$$

α is the progress variable of induction reaction, which decreases from unity in the induction reaction. β is the progress variable of exothermic reaction, which starts decreasing from unity when α goes below zero. The chemical reaction rates are expressed as:

$$\omega_\alpha=\frac{d\alpha}{dt}=-k_1\rho\exp(-E_1/RT) \tag{4}$$

$$\omega_\beta=\frac{d\beta}{dt}=\begin{cases}-k_2p^2\left[\beta^2\exp\left(\frac{-E_2}{RT}\right)-(1-\beta)^2\exp\left(-\frac{E_2+q}{RT}\right)\right] & (a\le 0)\\ 0 \quad (0<\alpha\le 1)\end{cases} \tag{5}$$

Where E_1, E_2, k_1, and k_2 are the parameters proposed by Korobeinikov et al. (1972) for the stoichiometric hydrogen-oxygen mixture at standard conditions ($T_0=292$ K, $p_0=1$ atm). In all the cases presented in this study, the inlet pressure and temperature are fixed at 1 atm and 292 K, respectively. The Steger–Warming splitting approach (Steger and Warming, 1981) is used to split the flux vectors. The fifth-order weighted essentially non-oscillatory (WENO) scheme (Jiang and Shu, 1996) is used to solve the splitted flux vectors. The third-order Runge–Kutta scheme is adopted to integrate the discretized equations in time.

A schematic of the computational domain is shown in Figure 2. The computational domain is represented by the rectangle above the wedge surface. The axes x and y are parallel and vertical to the wedge surface, respectively. At the left and upper boundaries, the inflow boundary conditions are fixed at the initial values. At the second part of the lower

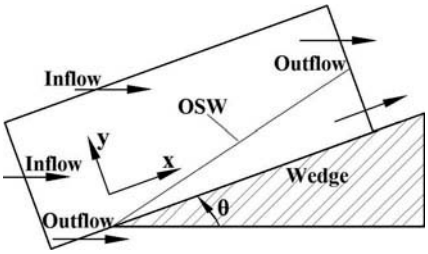

Figure 2 Schematic of the computational domain.

boundary (wedge surface), the slip boundary is adopted. The outflow conditions imposed to the right boundary and the first part of the lower boundary specify zero gradient for all variables. In all of the cases presented in this study, the wedge tip starts from the 20th grid point.

All the calculations presented in this study are performed using a uniform mesh in both directions, and the grid size Δx is fixed at 0.02 mm. About 18 computational cells are situated in the induction zone. In all of the results presented, the major structures and cellular structures are both well resolved with $\Delta x = 0.02$ mm. Furthermore, according to a comparison among the numerical results with Δx at 0.01 mm, 0.02 mm, and 0.04 mm, the major structures and cellular structures of the ODW at 0.02 mm are both mesh-independent.

RESULTS AND DISCUSSION

Initiation Process of an Upstream Propagating ODW

The initiation process of an upstream propagating ODW for the conditions of inflow Mach number $Ma_0 = 6.6$ and wedge angle $\theta = 26°$ is sequenced in Figure 3. The pressure fields at different times and the corresponding schematic figures are plotted. The OSW shown in Figure 2 is taken as the initial condition. The flow state ahead of the OSW is identical to that of the inflow. The flow state behind the OSW is identical to the one induced by the wedge in a non-reacting hydrogen-oxygen mixture. The hydrogen-oxygen mixture flows into the computational domain from the left and upper boundaries. At a fixed x coordinate, the induction time experienced by the gas decreases with the y coordinate, such that the exothermic reaction first starts at the smallest y coordinate. As shown in Figure 3a, the onset of combustion takes place in the vicinity of the wedge surface, and its position is determined by the induction process of the gas behind the OSW (Figueira da Silva and Deshaies, 2000). For instance, in the case presented in Figure 3, the length between the wedge tip and the onset position of combustion "B" is about 40 mm. This value is in good agreement with the induction length $L_{\text{R-H}}$ calculated with the flow state behind the OSW as the initial condition, which is about 39 mm. The induction length is given by $L_{\text{R-H}} = u_s\, t_i$, where u_s is the flow velocity behind the OSW and t_i is the induction time calculated with the flow state behind the OSW.

In Figure 3a, a half-round pressure wave appears above the wedge surface resulting from the onset of combustion. A similar phenomenon was also observed in the experiments performed by Maeda et al. (2013). Then the half-round pressure wave propagates towards the OSW and couples with it. Consequently, a curved ODW is established above the OSW as shown in Figures 3b and 3f. At the same time, a planar CJ ODW is formed at the end of the induction region. The ODW and the CJ ODW intersects at point "A," as shown in

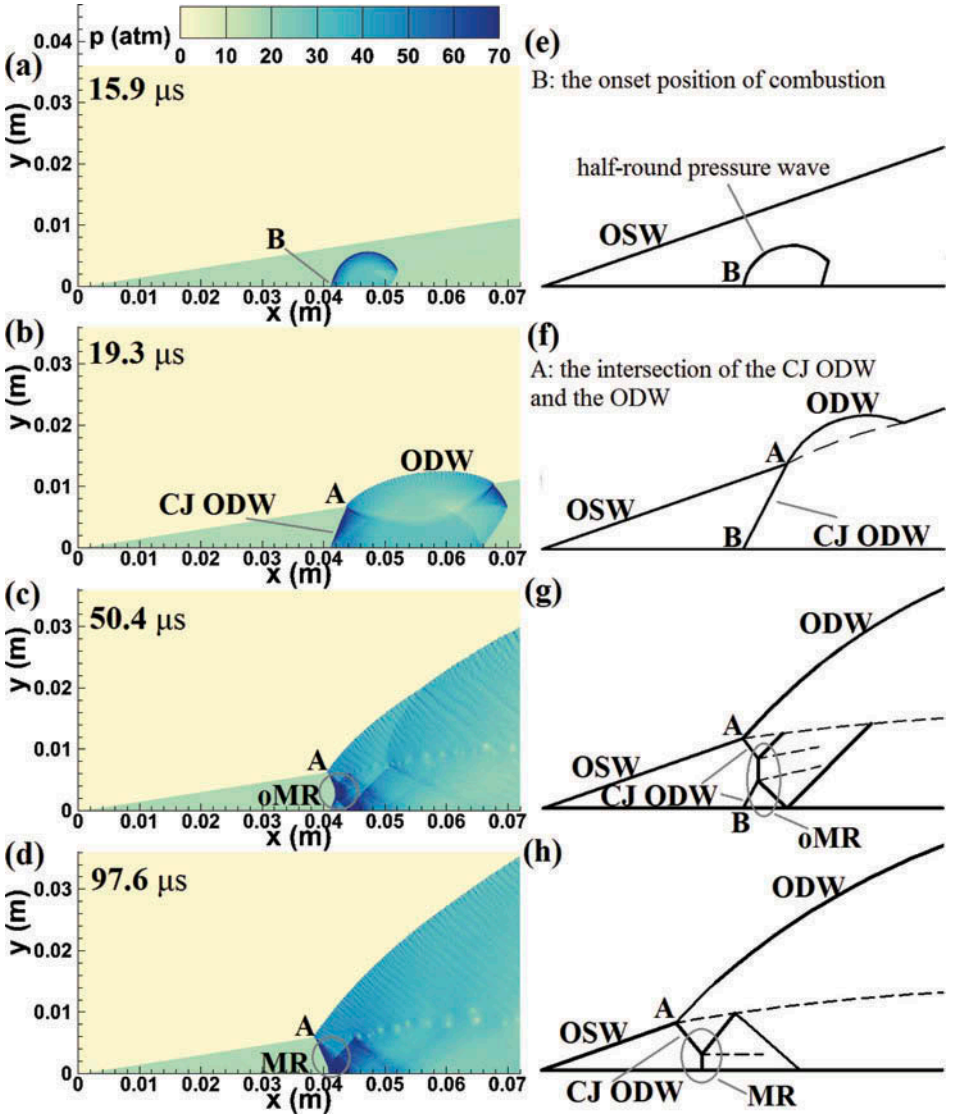

Figure 3 The initiation process of the upstream propagating ODW at $Ma_0 = 6.6$ and $\theta = 26°$. (a)–(d) The pressure fields of ODW at different times; (e)–(h) schematic figures.

Figures 3b and 3f. As observed in Figures 3b and 3c, the ODW does not stabilize at its initiation position. Instead, it propagates upstream (Figueira da Silva and Deshaies, 2000; Lefebvre and Fujiwara, 1995). As a result, the upper extreme point of the CJ ODW "A" propagates forward. Since the velocity of the CJ ODW remains constant, the wave front of it has to remain planar. Therefore, as shown in Figures 3c and 3g, the upper part of the CJ ODW folds forward to catch up with the upstream propagating ODW. Resulting from the interaction between the upper part and lower part of the CJ ODW, an overall Mach reflection (oMR) wave configuration is built up (Ben-Dor, 2007), as shown in Figures 3c and 3g. As the ODW propagates upstream, the oMR wave configuration moves towards the

wedge surface, and the lower triple point of the oMR eventually collides with the wedge surface. Consequently, as shown in Figure 3d, at $t = 97.6$ μs, a Mach reflection (MR) wave configuration is established, and the MR wave configuration persists during the upstream propagation of the ODW.

Mechanism of the Upstream Propagation of the ODW

In order to investigate the mechanism of the upstream propagation of the ODW, the R–H equations coupled with the exothermic reaction of the two-step combustion model (Korobeinikov et al., 1972) are solved. There are two assumptions: (1) the induction region is followed by a CJ ODW (Ghorbanian and Sterling, 1996); and (2) the gas behind the CJ ODW and ODW is in chemical equilibrium. Then the conservation laws of mass, momentum and energy, and the chemical equilibrium assumption yield:

$$\rho_0 u_{0n} = \rho_1 u_{1n} \tag{6}$$

$$(\rho_0 u_{0n}) u_{0t} = (\rho_1 u_{1n}) u_{1t} \tag{7}$$

$$p_0 + \rho_0 u_{0n}^2 = p_1 + \rho_1 u_{1n}^2 \tag{8}$$

$$h_0 + u_{0n}^2/2 = h_1 + u_{1n}^2/2 \tag{9}$$

$$\omega_\beta = 0 \tag{10}$$

where the subscripts 0 and 1 denote upstream and downstream conditions, respectively. The subscripts t and n denote the flow tangential and normal to the shock waves, respectively. With some manipulations presented by Pratt et al. (1991) and Ghorbanian and Sterling (1996), the final equations can be expressed as:

$$d\rho = \rho_0/\rho_1 = \tan(\beta_i - \theta_i)/\tan\beta_i \tag{11}$$

$$dp = p_1/p_0 = 1 + \gamma(Ma_0 \sin\beta_i)^2(1 - d\rho) \tag{12}$$

$$1 + (1 - \beta_{\text{eq}})Q - dp\, d\rho + \frac{\gamma - 1}{2}(Ma_0 \sin\beta_i)^2(1 - dp\, d\rho) = 0 \tag{13}$$

$$Q = q/(c_p T_0) \tag{14}$$

$$\beta_{\text{eq}} = \frac{1}{1 + \exp\left(\frac{q}{2RT_1}\right)} \tag{15}$$

where β_{eq} is the equilibrium value of the progress variable of exothermic reaction β, which is unity in the induction region. For the subscript $i = 1$, 2 and 3, β_i respectively denotes the angle of the OSW, CJ ODW, and ODW, as shown in Figure 1. θ_i denotes the flow deflection angle, which equals to θ for the OSW and ODW. For the CJ ODW, θ_i is obtained with the CJ assumption that the normal Mach number of the flow exiting the wave is unity.

Table 1 Summary of the analytical and numerical results

Ma_0	θ (°)	$\beta_{2,\text{R-H}}$ (°)	$\beta_{2,\text{num}}$ (°)	t_{num} (μs)	State[a]
6.2	25	77.0	69.0	101	P
6.4	25	71.0	66.0	120	P
6.6	25	66.7	65.9	277	P
6.6	26	69.3	66.5	79	P
6.6	27	72.5	68.4	29	P
6.6	28	76.8	68.6	14	P
6.8	25	63.2	62.3	—	S
6.8	27	68.1	66.4	47	P
7.0	25	60.4	59.6	—	S
7.0	27	64.6	66.4	133	P
7.2	25	57.9	57.5	—	S
7.2	27	61.7	60.0	—	S

[a]P: the ODW propagates upstream; S: the ODW stabilizes at its initiation position.

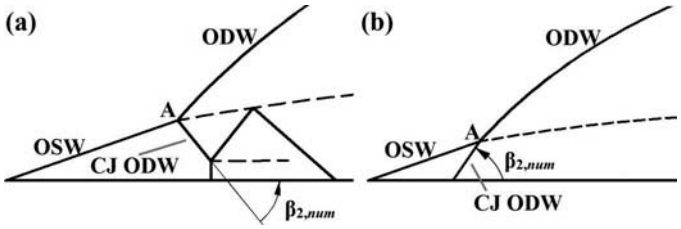

Figure 4 Schematic of the numerical result of the CJ ODW angle β_2. (a) $\beta_{2,\text{num}}$ for state "P"; (b) $\beta_{2,\text{num}}$ for state "S."

Table 1 is a summary of the key parameters obtained by R–H analysis and numerical simulations. "P" denotes that the ODW can propagate upstream from its initiation position in the numerical result. "S" denotes that the ODW can stabilize at its initiation position in the numerical result. In Table 1, $\beta_{2,\text{R-H}}$ and $\beta_{2,\text{num}}$ are the analytical and numerical results of the CJ ODW angle β_2, which is the angle between the CJ ODW and the wedge surface. Figure 4 shows the definitions of $\beta_{2,\text{num}}$ in these two conditions. When the ODW can stabilize at its initiation position, the CJ ODW angle obtained by numerical simulation $\beta_{2,\text{num}}$ is always in good agreement with the value obtained by R–H analysis $\beta_{2,\text{R-H}}$. Here, $\beta_{2,\text{R-H}} = \sin^{-1}(u_{\text{CJ}}/u_s)$, u_{CJ} is the velocity of the CJ ODW obtained with the flow state in the induction region as the initial condition. When the ODW can propagate upstream, $\beta_{2,\text{num}}$ is usually slightly smaller than the value of $\beta_{2,\text{R-H}}$. It results from the upstream propagation of the CJ ODW, which leads to the flow velocity relative to the CJ ODW slightly larger than u_s. However, the variation trends of the angles are the same. Therefore, the R–H analysis on the CJ ODW is reliable.

Figure 5 shows the wave angles β_1, β_2, and β_3 and the post-shock pressures p_{OSW}, $p_{\text{CJ ODW}}$, and p_{ODW} of the OSW, CJ ODW, and ODW versus θ of $Ma_0 = 6.6$. The results shown in Figure 5 are obtained by solving the above mentioned R–H relations. The values of θ at the detachment points of CJ ODW $\theta_{\text{det,CJ ODW}}$ and ODW $\theta_{\text{det,ODW}}$ are 29.2° and 29.9°. They are both greater than the value of $\theta = 26°$, adopted in the case of Figure 3. Thus, analytically, neither the CJ ODW nor the ODW shown in Figure 3 is detached. It is identical to the numerical results shown in Figures 3b and 3c that the lower part of the CJ

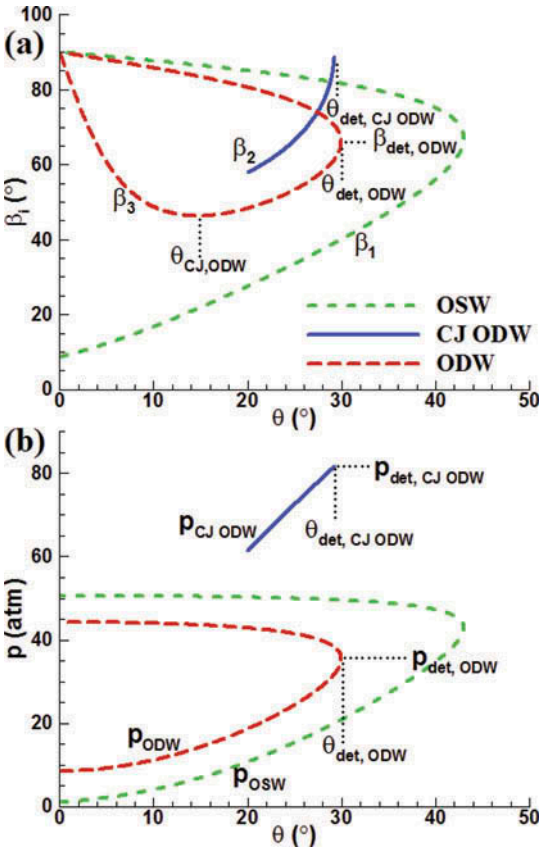

Figure 5 Shock polars at $Ma_0 = 6.6$. (a) Wave angle vs. wedge angle; (b) post-shock pressure vs. wedge angle.

ODW does not move forward before the oMR wave configuration is established. And in the following section, it will be found that in the numerical result the ODW itself is attached as well. In view of the fact that neither the ODW nor the CJ ODW can detach from its initiation position by itself, the upstream propagation of the ODW should result from the interaction between them.

To clarify the influence of the CJ ODW on the ODW, $p_{\text{CJ ODW}}$ and p_{ODW} of $Ma_0 = 6.6$ are plotted in Figure 5b. It is observed that $p_{\text{CJ ODW}}$ is always much higher than p_{ODW} and the detachment pressure of ODW$p_{\text{det,ODW}}$, 35.5 atm. The same phenomenon was also observed in the experiments conducted by Dabora and Broda (1993). Figure 6 is a close-up view of the pressure field of the upstream propagating ODW shown in Figure 3d. Figure 6a shows that the high pressure detonation products of CJ ODW are expanded through a centered expansion wave (CEW). Through the CEW, the pressure of the CJ ODW products is reduced. The expanded CJ ODW products and the ODW products are separated by a shear layer that cannot withstand any pressure difference. Figure 6b shows the pressure fields of the CJ ODW products ($y = 5$ mm) and the ODW products ($y = 8$ mm). The phenomenon shown in Figure 6b is qualitatively identical to the experimental pressure traces presented by Dabora and Broda (1993). It is observed in Figure 6b that the pressure of the expanded CJ ODW products is still higher than p_{ODW} and even $p_{\text{det,ODW}}$ at $Ma_0 = 6.6$ and $\theta = 26°$.

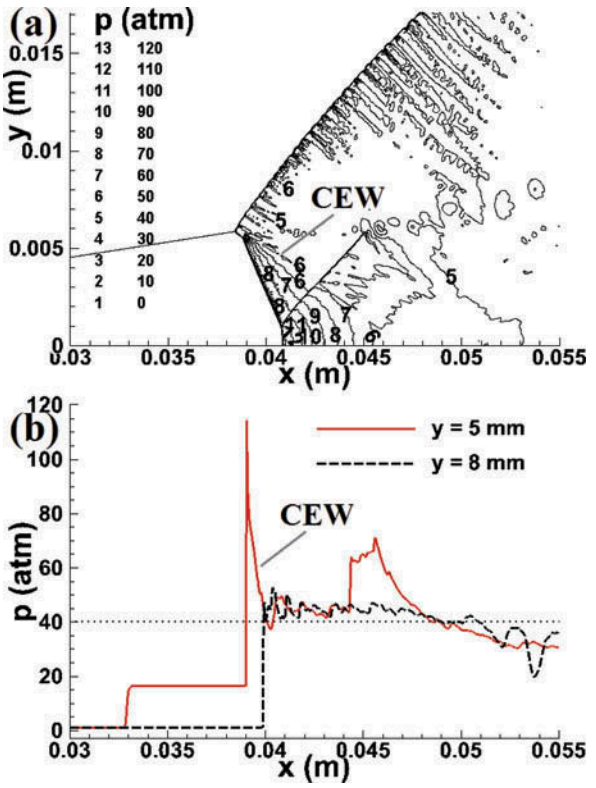

Figure 6 A close-up view of the pressure field of the upstream propagating ODW shown in Figure 3d. (a) Pressure contour near the CJ ODW; (b) pressure distribution along $y = 5$ mm and 8 mm.

To balance the pressure of the CJ ODW products, the ODW in the vicinity of the CJ ODW is strengthened. Geometrically, the ODW in the vicinity of the CJ ODW becomes convex and this phenomenon was also observed in the experimental results of Dabora and Broda (1993), Viguier et al. (1998), and Wang et al. (2011). As shown in Figure 6b, the pressure behind the convex ODW is higher than $p_{\mathrm{det,ODW}}$. Therefore, the ODW has to propagate upstream to match with the post-shock pressure.

To investigate the influence of the variation of Ma_0 and θ on the upstream propagation of the ODW, the pressure ratios η between $p_{\mathrm{CJ\,ODW}}$ and $p_{\mathrm{det,ODW}}$ for different Ma_0 versus θ are plotted in Figure 7. It is observed that η increases with θ and decreases with Ma_0. Therefore, analytically, the increase of θ and the decrease of Ma_0 are conducive to the upstream propagation of the ODW. This analysis is consistent with the numerical results. According to the states of the ODW at $\theta = 25°$ shown in Table 1, we find that only in the cases at low inflow Mach number $Ma_0 \leq 6.6$, the ODW can propagate upstream. In the cases at higher inflow Mach number $Ma_0 \geq 6.8$, the ODW stabilizes at its initiation position. A similar behavior is observed in the cases at $\theta = 27°$. By comparing the states of the ODW at $Ma_0 = 6.8$, we find that the ODW can propagate upstream at $\theta = 27°$. But it stabilizes at its initiation position at a smaller wedge angle $\theta = 25°$. A similar behavior is observed for the ODW at $Ma_0 = 7.0$. Therefore, it can be concluded that the decrease of Ma_0 and increase of θ are conducive to the upstream propagation of the ODW.

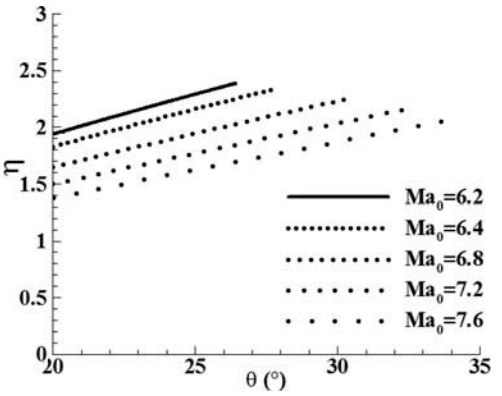

Figure 7 The ratio η between $p_{\mathrm{CJ\,ODW}}$ and $p_{\mathrm{det,ODW}}$ of different Ma_0.

Not only the issue of whether the ODW can propagate upstream from its initiation position is influenced by Ma_0 and θ, its upstream propagation process is also influenced by them dramatically. t_{num} listed in the fifth column of Table 1 is the time elapsed from the onset of combustion until the build-up of the MR wave configuration. It is observed that for the cases at $\theta = 25°$ and 27°, the time t_{num} increases dramatically with Ma_0. For example, the value of t_{num} for $Ma_0 = 6.6$ is 2.7 times of the value for $Ma_0 = 6.2$ at $\theta = 25°$. For the cases at $Ma_0 = 6.6$, the time t_{num} decreases dramatically with θ. For instance, the value of t_{num} for $\theta = 25°$ is 19.8 times of the value for $\theta = 28°$.

A typical upstream propagation process of ODW is sequenced in Figure 8. In this figure, the ODW propagates forward, and the length of the CJ ODW decreases. Meanwhile, the size of the convex ODW decreases. In other words, the area of the high pressure region behind the ODW decreases with its upstream propagation. Therefore, the influence of the CJ ODW on the ODW becomes progressively weaker. If the ODW propagates to the tip of the wedge, the CJ ODW will vanish and its influence on the ODW will vanish as well. Thus, if the ODW cannot detach from the wedge surface by itself, it will have to stabilize on the wedge surface. Due to the thermoneutrality of the induction process, a new induction region will be established in the vicinity of the wedge tip. The pressure field of a stabilized upstream propagating ODW is shown in Figure 9. The values of the wave angle of the stabilized upstream propagating ODW shown in Figures 8 and 9 are 55.3° and 52.9°, respectively. They are in good agreement with the corresponding values obtained by R–H analysis, namely, 54.4° and 52.7°.

The length L_{num} of the new induction region of the stabilized upstream propagating ODW is always approximately several millimeters, a few times that of the induction zone of an ideal ZND detonation L_i, as shown in Figure 9b. It is about one order of magnitude shorter than the induction length $L_{\mathrm{R\text{-}H}}$ determined by the flow state behind the OSW. For example, for $\theta = 27°$ and $Ma_0 = 6.6$, 6.8, and 7.0, the nondimensional induction region length L_{num}/L_i is 1.9, 2.7, and 6.0, respectively. In these three cases, $L_{\mathrm{num}}/L_{\mathrm{R\text{-}H}}$ is 0.028, 0.056, and 0.17, respectively. Similar characteristics are also observed for the cases at $\theta = 25°$, 26°, and 28°. Even taking the influence of the boundary layer into account, according to Li et al. (1993), the length of the induction region will not become longer. Because the flow behind the ODW is always supersonic, the wedge used to sustain such an ODW can be significantly reduced. It is a very desirable feature for propulsion applications, since a shorter wedge means reduced drag.

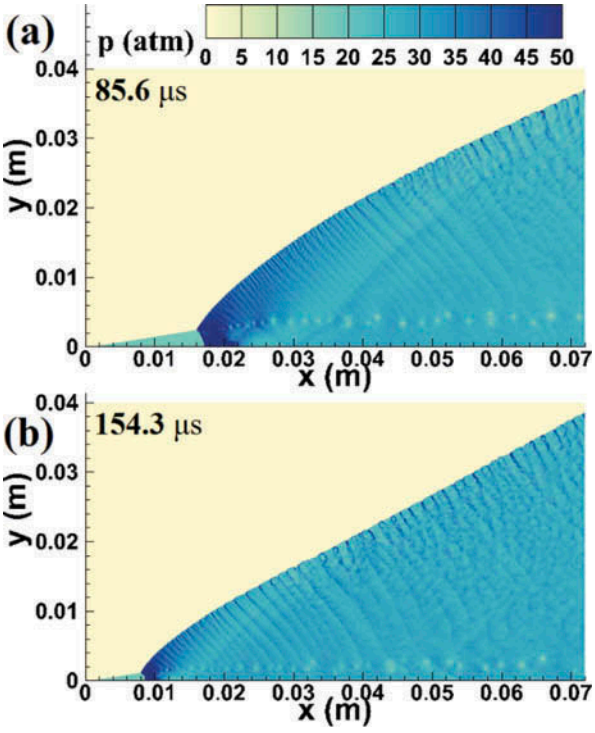

Figure 8 Temporal evolution of the pressure filed of the upstream propagating ODW at $Ma_0 = 6.8$ and $\theta = 27°$. (a) $t = 85.6$ μs; (b) $t = 154.3$ μs.

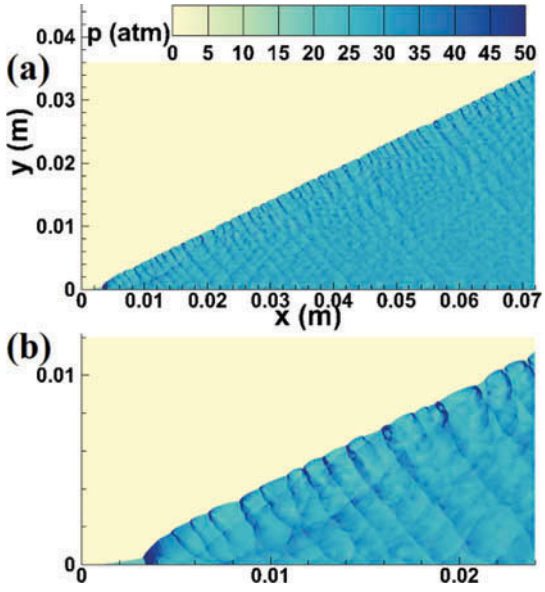

Figure 9 (a) Pressure field and (b) its close-up view of the stabilized upstream propagating ODW at $Ma_0 = 7.0$ and $\theta = 27°$.

Stability of the Stabilized Upstream Propagating ODW

The stability of the ODW at high and critical inflow Mach number has been confirmed by Li et al. (1994) and Teng et al. (2007), respectively. We now perform an investigation of the stability of the stabilized upstream propagating ODW. In the simulations, disturbances with T_0 increased to 500 K are artificially introduced into the stabilized solution for the case of $Ma_0 = 7.0$ and $\theta = 27°$, as shown in Figures 10a and 10d. In the first case, the high temperature region interacts with both the induction region and the ODW. In the second case, the high temperature region only interacts with the ODW.

As shown in Figures 10b and 10e, the ODW is strengthened when the high temperature region interacts with it in both cases. But the disturbance is convected out of the ODW front in just a few microseconds. Although the induction region is disturbed in the first case, the ODW is not disturbed severely as in the cases of high and critical inflow Mach number (Li et al., 1994; Teng et al., 2007). This behavior should result from the small size of the induction region of the stabilized upstream propagating ODW. As the induction region is much smaller than that of the high and critical inflow Mach number, the disturbance resulting from premature ignition in the induction region is much smaller as well. Accordingly, the large disturbance starts from the induction region, presented in the work of Li et al. (1994) and Teng et al. (2007), does not occur here. Therefore, it can be concluded that the stabilized upstream propagating ODW is more stable than a wave that remains at its initiation position.

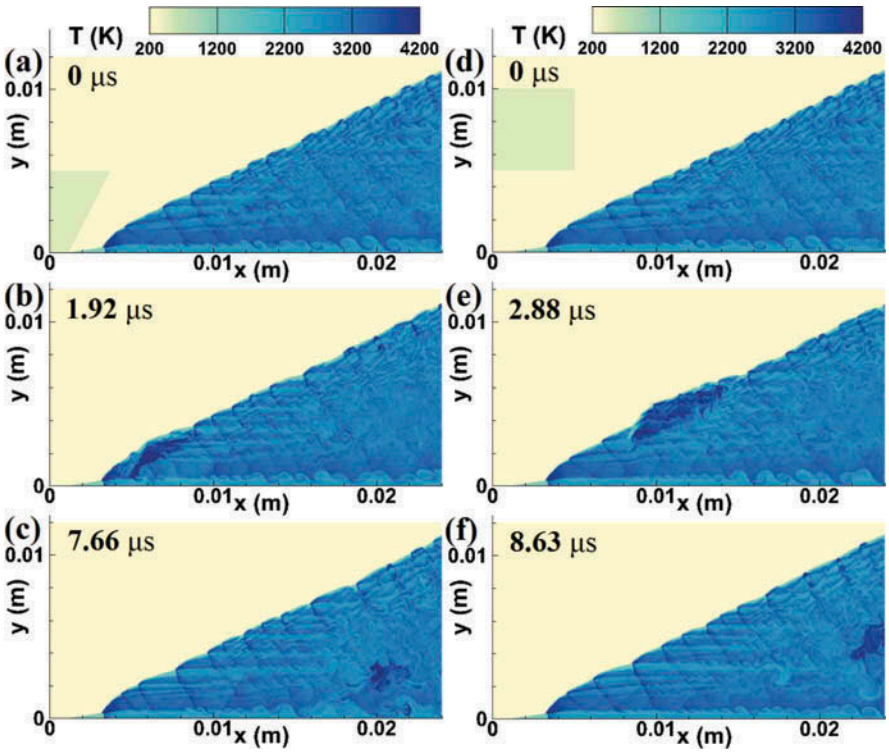

Figure 10 Temporal evolution of the disturbance in the stabilized upstream propagating ODW at $Ma_0 = 7.0$ and $\theta = 27°$.

CONCLUSIONS

1. The ODW at low inflow Mach number is analytically and numerically investigated via R–H analysis and two-dimensional numerical simulations. It is found that the CJ ODW has a strengthening influence on the ODW. The influence of the CJ ODW is the reason why an attached ODW can propagate upstream.
2. Both analytical and numerical results show that the decrease of inflow Mach number and the increase of wedge angle are conducive to the upstream propagation of the ODW.
3. A MR wave configuration is always established on the wedge surface in the upstream propagation process of the ODW. The time needed to build up such a MR wave configuration from the onset of combustion increases with the inflow Mach number and decreases with the wedge angle.
4. For the cases of an ODW that cannot detach from the wedge surface by itself, the ODW will stabilize at a point on the wedge surface. An induction region, which is a few times the length of the induction zone of an ideal ZND detonation, will be established. Thus, the wedge needed to sustain it can be very short. Consequently, the drag induced by the wedge can be reduced. This drag reduction is a very desirable feature for the propulsion applications of ODW.
5. Benefiting from the short induction region, the stabilized upstream propagating ODW has extraordinary stability.

ACKNOWLEDGMENT

The authors greatly appreciate the useful and important comments from Yi-Ning Zhang.

FUNDING

This work is supported by Science and Technology on Scramjet Laboratory, the 31st Research Institute of CASIC.

REFERENCES

Ashford, S.A., and Emanuel, G. 1994. Wave angle for oblique detonation waves. *Shock Waves*, **3**, 327–329.

Ben-Dor, G. 2007. *Shock Wave Reflection Phenomena*, 2nd edn., Springer-Verlag, New York, pp. 90–95.

Brackett, D.C., and Bogdanoff, D.W. 1989. Computational investigation of oblique detonation ramjet-in-tube concepts. *J. Propul. Power*, **5**, 276–281.

Cambier, J.L., Adelman, H., and Menees, G.P. 1988. Numerical simulations of an oblique detonation wave engine. AIAA-88-0063. Presented at the AIAA 26th Aerospace Sciences Meeting, Reno, NV, January 11–14.

Choi, J.-Y., Shin, E.J.-R., and Jeung, I.-S. 2009. Unstable combustion induced by oblique shock waves at the non-attaching condition of the oblique detonation wave. *Proc. Combust. Inst*., **32**, 2387–2396.

Dabora, E.K., and Broda, J.-C. 1993. Standing normal detonations and oblique detonations for propulsion. AIAA Paper, AIAA-93-2325.

Desbordes, D., Hamada, L., and Guerraud, C. 1995. Supersonic H_2-air combustions behind oblique shock waves. *Shock Waves*, **4**, 339–345.

Dudebout, R., Sislian, J.P., and Oppitz, R. 1998. Numerical simulation of hypersonic shock-induced combustion ramjets. *J. Propul. Power*, **14**, 869–879.

Figueira da Silva, L.F., and Deshaies, B. 2000. Stabilization of an oblique detonation wave by a wedge: a parametric numerical study. *Combust. Flame*, **121**, 152–166.

Ghorbanian, K., and Sterling, J.D. 1996. Influence of formation processes on oblique detonation wave stabilization. *J. Propul. Power*, **12**, 509–517.

Grismer, M.J., and Powers, J.M. 1995. Calculations for steady propagation of a generic ram accelerator configuration. *J. Propul. Power*, **11**, 105–111.

Gui, M.-Y., Fan, B.-C., and Dong, G. 2011. Periodic oscillation and fine structure of wedge-induced oblique detonation waves. *Acta Mech. Sin*., **27**, 922–928.

Jiang, G.-S., and Shu, C.-W. 1996. Efficient implementation of weighted ENO schemes. *J. Comput. Phys*., **126**, 202–228.

Korobeinikov, V.P., Levin, V.A., Markov V.V., and Chernyi, G.G. 1972. Propagation of blast wave in a combustion gas. *Astronaut. Acta*, **17**, 529–537.

Lefebvre, M.H., and Fujiwara, T. 1995. Numerical modeling of combustion processes induced by a supersonic conical blunt body. *Combust. Flame*, **100**, 85–93.

Li, C., Kailasanath, K., and Oran, E.S. 1993. Effects of boundary layers on oblique-detonation structures. AIAA Paper, AIAA-93-0450.

Li, C., Kailasanath, K., and Oran, E.S. 1994. Detonation structures behind oblique shocks. *Phys. Fluids*, **6**, 1600–1611.

Maeda, S., Kasahara, J., and Matsuo, A. 2012. Oblique detonation wave stability around a spherical projectile by a high time resolution optical observation. *Combust. Flame*, **159**, 887–896.

Maeda, S., Sumiya, S., Kasahara, J., and Matsuo, A. 2013. Initiation and sustaining mechanisms of stabilized oblique detonation waves around projectiles. *Proc. Combust. Inst*., **34**, 1973–1980.

Morris, C.I., Kamel, M.R., and Hanson, R.K. 1998. Shock-induced combustion in high-speed wedge flows. *Proc. Combust. Inst*., **27**, 2157–2164.

Papalexandris, M.V. 2000. A numerical study of wedge-induced detonations. *Combust. Flame*, **120**, 526–538.

Pratt, D.T., Humphrey, J.W., and Glenn, D.E. 1991. Morphology of standing oblique detonation waves. *J. Propul. Power*, **7**, 837–845.

Steger, J.L., and Warming, R.F. 1981. Flux vector splitting of the inviscid gasdynamic equations with application to finite-difference methods. *J. Comput. Phys*., **40**, 263–293.

Teng, H.-H., Zhao, W., and Jiang, Z.-L. 2007. A novel oblique detonation structure and its stability. *Chin. Phys. Lett*., **24**, 1985–1988.

Verreault, J., and Higgins, A.J. 2011. Initiation of detonation by conical projectiles. *Proc. Combust. Inst*., **33**, 2311–2318.

Verreault, J., Higgins, A.J., and Stowe, R.A. 2012. Formation and structure of steady oblique and conical detonation waves. *AIAA J*., **50**, 1766–1772.

Verreault, J., Higgins, A.J., and Stowe, R.A. 2013. Formation of transverse waves in oblique detonations. *Proc. Combust. Inst*., **34**, 1913–1920.

Viguier, C., Figueira da Silva, L.F., Desbordes, D., and Deshaies, B. 1996. Onset of oblique detonation waves: Comparison between experimental and numerical results for hydrogen-air mixtures. *Proc. Combust. Inst*., **26**, 3023–3031.

Viguier, C., Gourara, A., and Desbordes, D. 1998. Three-dimensional structure of stabilization of oblique detonation wave in hypersonic flow. *Proc. Combust. Inst*., **27**, 2207–2214.

Wang, A.-F., Zhao, W., and Jiang, Z.-L. 2011. The criterion of the existence or inexistence of transverse shock wave at wedge supported oblique detonation wave. *Acta Mech. Sin*., **27**, 611–619.